Original research

Levistilide A inhibits angiogenesis in liver fibrosis via vascular endothelial growth factor signaling pathway

Zhi-Min Zhao[1,2], Hong-Liang Liu[1], Xin Sun[1], Tao Guo[1], Li Shen[1], Yan-Yan Tao[1] and Cheng-Hai Liu[1,2,3]

[1]Institute of Liver Diseases, Shuguang Hospital affiliated to Shanghai University of Traditional Chinese Medicine, Shanghai 201203, China; [2]Shanghai Key Lab of Liver Diseases of TCM, Shanghai 201203, China; [3]E-Institute of TCM Internal Medicine, Shanghai Municipal Education Commission, Shanghai 201203, China

Corresponding author: Cheng-Hai Liu. Email: chenghailiu@hotmail.com

Impact statement

Levistilide A has been reported to inhibit hepatic stellate cell (HSC) proliferation. In this study, we further investigated the mechanisms of levistilide A on liver fibrosis relating to angiogenesis, particularly on the characteristic change in liver sinusoidal endothelial cells. The cell models of HSC and liver sinusoidal endothelial cell and CCl_4 induced liver fibrosis model were used. These results suggest that levistilide A can inhibit liver fibrosis through antiangiogenesis by alleviating sinusoid capillarization via the vascular endothelial growth factor signaling pathway. The effect of levistilide A on liver fibrosis was confirmed, and its detailed mechanism was also discussed. These findings suggest that levistilide A may be a great potential drug for treating liver fibrosis through antiangiogenesis, and this effect will be verified in other fibrotic animal model studies or by clinical trials.

Abstract

Levistilide A ($C_{24}H_{28}O_4$, molecular weight = 380.48) derived from *Angelica sinensis* (Danggui) has been reported to inhibit hepatic stellate cell proliferation. This study investigated the effects of levistilide A on liver fibrosis relating to angiogenesis, particularly on the characteristic change in liver sinusoidal endothelial cells. LX-2 cells were activated by TGF-β1, and the human hepatic sinusoidal endothelial cells (HHSECs) were induced by endothelial cell growth supplement. Cell viability was detected using a methylthiazoldiphenyl–tetrazolium bromide assay; F-actin was visualized through the fluorescence probe method; cell proliferation was examined using the EdU kit; antiangiogenesis activity was assessed using the tube formation assay and transgenic zebrafish model. To verify the results *in vivo*, rats were subcutaneously injected with CCl_4 twice a week for six weeks to duplicate the liver fibrosis model and then treated with 10 mL/kg of normal saline, 4 mg/kg of sorafenib, and 3 and 6 mg/kg of levistilide A for three weeks from the fourth week. Collagen deposition was detected through Sirius Red staining; liver microvasculature was examined through vWF labeling and X-ray 2D imaging; sinusoidal fenestrations were observed through scanning electron microscopy; collagen I, α-SMA, CD31, vascular endothelial growth factor (VEGF), and VEGF-R2 were detected through Western blotting. Our results indicated that levistilide A attenuated LX-2 cell activation and HHSEC proliferation. The ability of HHSECs to form tubelike structures in Matrigel was inhibited, and the number of functional vessels in transgenic zebrafish decreased. In *in vivo* experiments, levistilide A reduced collagen deposition and the number of new microvessels; ameliorated sinusoid capillarization; and downregulated the expression of CD31, VEGF, and VEGF-R2. These findings suggest that levistilide A can inhibit liver fibrosis through antiangiogenesis by alleviating sinusoid capillarization via the VEGF signaling pathway.

Keywords: Liver fibrosis, angiogenesis, hepatic sinusoidal endothelial cell, capillarization, vascular endothelial growth factor signaling pathway, levistilide A

***Experimental Biology and Medicine* 2017; 242: 974–985. DOI: 10.1177/1535370217701005**

Introduction

Liver fibrosis commonly occurs in various chronic liver diseases and may advance to end-stage liver disease, cirrhosis, and even hepatocellular carcinoma.[1] Hepatic stellate cell (HSC) activation plays a key role in liver fibrosis and contributes to overdeposition of the extracellular matrix (ECM). However, angiogenesis occurs before fibrogenesis and promotes HSC activation and fibrosis development.[2] Sinusoidal capillarization with fenestration reduced or disappeared in liver sinusoidal endothelial cells (LSECs), and a continuous basement membrane is one of the major forms of angiogenesis in the liver. Furthermore, neovascularization and abnormalities in the angioarchitecture are closely related to progressive fibrogenesis.[3] Several experimental and clinical studies have demonstrated that angiogenesis and fibrogenesis have some common pathological

mechanisms and pathways, particularly the vascular endothelial growth factor (VEGF), platelet-derived growth factor (PDGF), transforming growth factor-β1 (TGF-β1), and fibroblast growth factor signaling pathways.[3] Antiangiogenesis is considered a target for fibrosis therapy. Sorafenib, a tyrosine kinase inhibitor, has been reported to inhibit vascular remodeling and have active effects on chronic liver diseases,[4] indicating that antiangiogenic treatment is a promising therapeutic approach for liver cirrhosis and related complications. However, no effective antiangiogenic agents are currently available.

Levistilide A is an active compound extracted from *Angelica sinensis* (Danggui). Danggui invigorates blood circulation and hence is considered as an efficient herb to treat chronic liver diseases. Previous research indicates that levistilide A can inhibit HSC proliferation activated by PDGF-BB through cell cycle inhibition and apoptosis.[5] Because LSEC plays a crucial role in HSC activity contributing to angiogenesis which are closely related to liver fibrosis, we aimed to evaluate the effect of levistilide A on angiogenesis from the cell level to the whole animal level and investigate the underlying mechanism, in particular, relating to sinusoid capillarization and VEGF signaling.

Materials and methods

Drug

Levistilide A ($C_{24}H_{28}O_4$, molecular weight = 380.48, purity ≥ 98%) was obtained from Shanghai Winherb Medical Technology Co., Ltd (Shanghai, China). Sorafenib was purchased from Bayer Healthcare Co., Ltd (Leverkusen, Germany).

Reagents

CCl_4 and olive oil were provided by Sinopharm Chemical Reagent Co., Ltd (Shanghai, China). The index kits of serum liver function including alanine aminotransamine (ALT), aspartate transamine (AST), albumin (Alb), and total bilirubin (TBil) were provided by Nanjing Jiancheng Bioengineering Institute (Nanjing, China). The primary antibody information included in the experiments are presented in Table 1. Secondary antibodies labeled with fluorescence and DAPI were purchased from RiboBio Co. Ltd (Guangzhou, China). Recombinant human TGF-β1 was obtained from R&D Systems, Inc. (Minneapolis, MN, USA). BD Matrigel™ Basement Membrane Matrix was purchased from BD Biosciences (Bedford, MA, USA).

Cell culture

LX-2 cell line was established by Prof. Lieming Xu and cultured in Dulbecco's modified eagle medium containing 10% fetal bovine serum (FBS). Human hepatic sinusoidal endothelial cells (HHSECs; Sciencell™ Research Laboratories, Carlsbad, CA, USA) were cultured in endothelial cell medium, which was supplemented with 5% FBS and 5% endothelial cell growth supplement (ECGS, provided by the manufacturer).

Drug treatments

Sorafenib and levistilide A were dissolved in serum-free medium containing 0.1% dimethyl sulfoxide (DMSO). For evaluating the toxicity of levistilide A, cells were adjusted to 8×10^4 cells/mL, and added 100 μL per well in 96-well plate, after serum starved, then incubated in conditioned media of levistilide A (0–100 μM) for 24 h (LX-2 cell) or for 48 h (HHSECs). Cell viability was detected using a methylthiazoldiphenyl–tetrazolium bromide (MTT; Sigma-Aldrich, St Louis, USA) assay. To assess LX-2 cell activation, cells were split into six groups: the DMSO group, TGF-β1 group, TGF-β1 + sorafenib (2.5 ng/mL) group, and TGF-β1 + levistilide A (12.5, 25, and 50 μM) groups, and the concentration of TGF-β1 was 2.5 ng/mL. After serum starving for 24 h, cells were incubated in the appropriate agent-conditioned medium for 24 h and labeled using Actin-Tracker Green (Beyotime, Shanghai, China) at 1:100 dilution ratio for measuring actin expression. Cell nuclei were stained with DAPI for 1 min[6] and analyzed using Cellomics ArrayScan VTI HCS reader (Thermo Fisher Scientific, Waltham, MA, USA). For the HHSEC proliferation experiment, after serum starving for 24 h, cells were split into six groups: the control group, the ECGS (2% v/v) group, the ECGS (2% v/v) + sorafenib (2.5 ng/mL) group, and the ECGS (2% v/v) + levistilide A (6.25, 12.5, and 25 μM) groups. After treatment with drugs for 48 h, cell proliferation was examined using a Cell-Light™ EdU Apollo®488 In Vitro Imaging Kit (RiboBio, Guangzhou, China), according to the operating instruction manual.

Table 1 Antibodies used in the study

Antibodies	Isotype	Suppliers	Cat. No.	Dilution
vWF	Rabbit polyclonal IgG	Abcam	ab6994	1: 200
Col I	Rabbit polyclonal IgG	Abcam	ab34710	1: 500
α-SMA	Rabbit polyclonal IgG	Abcam	ab5694	1: 500
CD31	Mouse monoclonal IgG1	Abcam	ab24590	1: 500
VEGF	Rabbit polyclonal IgG	Abcam	ab46154	1: 500
VEGF-R2	Rabbit polyclonal IgG	Abcam	ab39638	1: 500
GAPDH	Mouse Monoclonal	KangChen	KC-5G4	1: 5000

Tube formation assay

HHSECs were dispersed in the respective drug conditioned media and seeded in a 96-well plate coated with Matrigel, 1×10^4 cells per well, and incubated at 37°C with 5% CO_2 for 24 h according to the manufacturer's operating procedures. Three replicates were created for each group. Images of each well were captured using an IX83 inverted fluorescence microscope equipped with a DP71 digital camera (Olympus, Tokyo, Japan).

Transgenic zebrafish

Embryo manipulation. Embryos of zebrafish were selected under an integrated microscope, after 24 h of fertilization and moved to a 96-well plate with conditioned medium. Five replicates were created for each concentration. Negative control was prepared using the same volume of co-solvent. Subsequently, the plates were covered and placed into a light incubator at 28°C for 48 h. The blood cells migrating through the intersegmental vessels (ISVs) were counted under an inverted microscope, and zebrafish larvae were hatched from viable embryos. After narcotization by Tricaine, ISVs were observed under a fluorescence microscope. Alkaline phosphatase staining: 4% paraformaldehyde fixed embryos were dehydrated in methanol, permeabilized with acetone, washed twice in phosphate buffer, and balanced in NTMT buffer. NBT and BCIP staining solutions were added into the plate well. When all zebrafish embryos were stained, PBST was added to terminate the reaction.

Animal experimental design

Fifty male Wistar rats weighing 150–170 g were purchased from Shanghai Laboratory Animal Center of Chinese Academy of Sciences (Shanghai, 2007-005). The animals were housed under a reverse 12 h light/dark cycle condition. We followed the international guidelines for the use and care of laboratory animals. The animals were randomly divided into five groups: normal control ($n = 10$), CCl_4 model control ($n = 10$), CCl_4 + sorafenib ($n = 10$), CCl_4 + 3 mg levistilide A ($n = 10$), CCl_4 + 6 mg levistilide A ($n = 10$). Except the rats in the normal control group, rats in the other four groups were fed with high-lipid and low-protein diets containing 79.5% corn flour, 20% lard, and 0.5% cholesterol for two weeks, and subsequently with pure corn flour for four weeks. First, 5 mL/kg of 100% CCl_4 was subcutaneously injected followed by 3 mL/kg of 40% CCl_4–olive oil solution twice a week for six weeks.[7] From the fourth week, the four groups were given 10 mL/kg of normal saline (model group), intragastric injection of 4 mg/kg of sorafenib (sorafenib group), intraperitoneal injection of 3 mg/kg of levistilide A (3 mg/kg levistilide A group), and 6 mg/kg of levistilide A (6 mg/kg levistilide A group) daily for three weeks. Rats in the control group received a normal diet with no CCl_4 for six weeks.

Pathological examination

For Sirius Red staining, liver tissues fixed in 4% formaldehyde and dehydrated in alcohol were embedded in paraffin and sectioned into 4-μm-thick specimens. Slides were stained with Sirius Red to assess collagen deposition. For synchrotron radiation X-ray 2D imaging, the dehydrated liver specimens were imaged at BL13W beamline in Shanghai Synchrotron Radiation Facility (Shanghai, China), the third-generation synchrotron source. The experimental parameters used were as follows: 34 keV energy, 1 m sample–detector distance, and 50 ms/frame exposure time. For ultrastructure analysis, after perfusion with phosphate buffered saline (PBS) and 2.5% glutaraldehyde successively through the portal vein, 3-mm-thick slices were cut from the livers for scanning electron microscopy (SEM), and 1-mm^3 cubic liver samples were harvested for transmission electron microscopy (TEM). The tissues were fixed in 2.5% glutaraldehyde at 4°C for 48 h. All experiments were performed in the electron microscopy room of the Shanghai University of Traditional Chinese Medicine.

Immunofluorescence

Seven-micrometer-thick frozen sections of liver tissue were fixed in cold acetone for 10 min, washed with PBS, and blocked with 0.2% bovine serum albumin for 1 h at 37°C. Specific primary antibodies were incubated overnight at 4°C, fluorescein isothiocyanate-labeled secondary antibodies were incubated for 1 h at 37°C, and DAPI-stained nucleus was incubated for 1 min. The tissues were observed through confocal microscopy, and images were captured through the Olympus confocal software. The primary antibody of negative control was replaced with PBS. All samples of liver tissue were observed. Microvessel density of liver tissue in CCl_4 rats was calculated as the mean number of von Willebrand factor (vWF)-labeled vessels in randomly selected five high magnification fields per section (×400) using the Image-Pro Plus software.[7]

Western blot analyses

According to the reported process,[8] samples were lysed in the radioimmunoprecipitation assay buffer (150 mM NaCl, 1% NP-40, 0.1% SDS, 50 mM Tris–HCl, pH 7.4, 1 mM EDTA, 1 mM PMSF, 1 × complete mini protease inhibitor cocktail) and centrifuged for 10 min at 10,000 × g and 4°C for 15 min. The supernatant was collected and protein was measured using a bicinchoninic acid Protein Assay Kit (Thermo, Rockford, IL, USA). Protein was separated through 10% sodium dodecyl sulfate-polyacrylamide gel electrophoresis and transferred onto a nitrocellulose membrane. After blocking with 5% non-fat milk in TBST at room temperature for 1 h, the membrane was incubated with the primary antibody at 4°C overnight and subsequently with secondary antibody at room temperature for 1 h. Signals were visualized using the ECL kit (Upstate Biotechnology, Lake Placid, NY, USA) and measured using a Chemi Doc image analyzer (Bio-Rad, Hercules, CA, USA).

Statistical analysis

All data are presented as mean ± standard deviation. The difference between the groups was analyzed using one-way

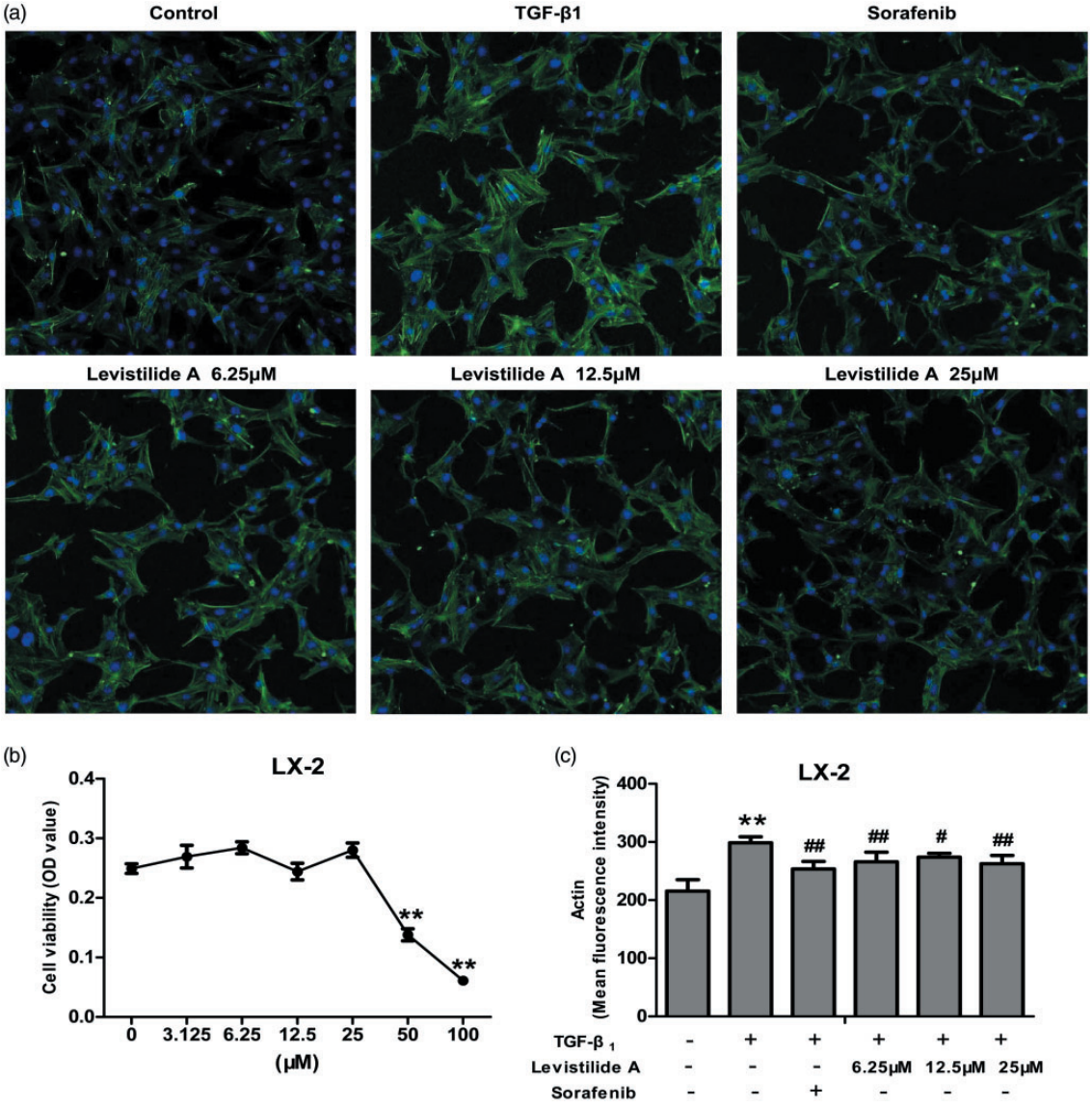

Figure 1 Levistilide A inhibited TGF-β1-induced LX-2 cell activation. (a) Cells were incubated with 2.5 ng/mL TGF-β1 with or without levistilide A for 24 h. Sorafenib (2.5 ng/mL) was used as a positive control. Cells were labeled using Actin-Tracker Green and scanned using Cellomics ArrayScan VTI HCS reader (×100). (b) Influence of levistilide A on the viability of LX-2 cells (MTT assay). LX-2 cells were incubated with 6.25, 12.5, and 25 μM levistilide A for 24 h, and cell viability was evaluated to define the maximum dose without toxicity. The maximum dose without toxicity was 25 μM, and hence, doses < 25 μM were applied in the following experiments. (c) Effects of levistilide A on LX-2 activation were measured by the mean fluorescence intensity of actin. $^{**}P < 0.01$, compared with normal control. $^{\#}P < 0.05$, $^{\#\#}P < 0.01$, compared with model control. The experiments were repeated three times. (A color version of this figure is available in the online journal.)

ANOVA performed with SPSS 15.0 software. Statistical significance was determined at $P < 0.05$.

Results

Levistilide A inhibited TGF-β1-induced LX-2 cell activation

Cell toxicity results showed that LX-2 cell viabilities were significantly reduced by levistilide A at a concentration from 25 to 100 μM (Figure 1(b)). Thus, the maximum dose without toxicity was 25 μM. Therefore, a concentration up to 25 μM was used in the following experiments. LX-2 activation was induced by TGF-β1 (2.5 ng/mL) for 24 h. The results showed that levistilide A and sorafenib significantly inhibited the mean fluorescence intensity of actin (Figure 1(a) and (c)), thus indicating that levistilide A and sorafenib inhibited LX-2 cell activation. The results correspond with the report of literatures.

Levistilide A attenuated ECGS-induced HHSEC proliferation

Cell toxicity results showed that HHSEC viabilities were not significantly reduced by levistilide A within a concentration of 100 μM (Figure 2(b)); a concentration within 25 μM was selected for the following experiments consistent with LX-2. The HHSEC proliferation model was induced by ECGS for 48 h. Model cells showed an increase in the

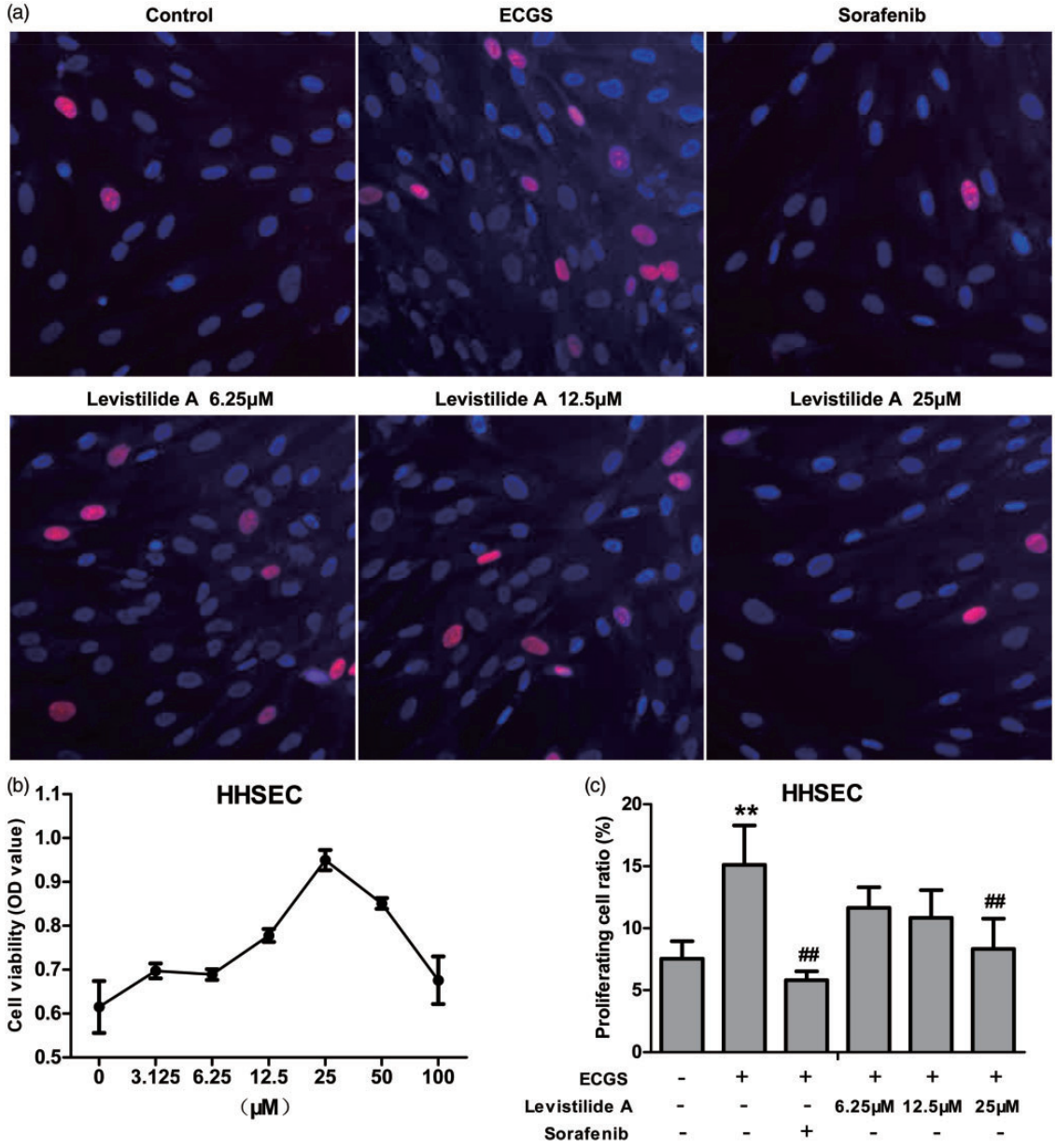

Figure 2 Levistilide A attenuated ECGS-induced HHSEC proliferation. (a) HHSEC proliferation was induced by ECGS. Cells were treated with various concentrations of levistilide A for 24 h. After co-incubation with EdU dye and nucleus labeling with DAPI, HHSECs were scanned using Cellomics ArrayScan VTI HCS reader (×200). (b) Influence of levistilide A on the viability of HHSECs (MTT assay). HHSECs were incubated with various concentrations of levistilide A for 24 h, and cell viability was evaluated to define the maximum dose without toxicity. The maximum dose without toxicity was 100 μM, and hence, doses < 25 μM were applied in the following experiments. (c) The proliferating cell ratio of EdU positive cell and total cell number was calculated. $^{*}P < 0.05$, $^{**}P < 0.01$, compared with normal control. $^{\#\#}P < 0.01$, compared with model control. The experiments were repeated three times. (A color version of this figure is available in the online journal.)

proliferating cell ratio (Figure 2(a) and (c)), which reduced significantly after levistilide A treatment (6.26, 12.5, and 25 μM). Similar effects were observed in the sorafenib group.

Levistilide A inhibited the HHSEC tube formation in Matrigel

Tube formation assay was performed to test the ability of HHSECs to form tubules. HHSECs cultured without Matrigel were present in the form of individual cells or flat cells at 24 h, and those cultured in Matrigel formed tubelike structures. HHSECs were elongated and interconnected, resulting in the formation of a tightly adherent tubular network. Sorafenib (2.5 ng/mL) and levistilide A (6.25, 12.5, and 25 μM) inhibited tube formation, and also the cluster of cells significantly reduced after treatment with 25 μM of levistilide A (Figure 3(a)). These findings suggested that levistilide A inhibited the ability of HHSECs to form tubelike structures in Matrigel.

Levistilide A inhibited the number of functional vessels in transgenic zebrafish

Toxic manifestations such as no blood flow, yolk sac edema, and tail up were observed in levistilide A

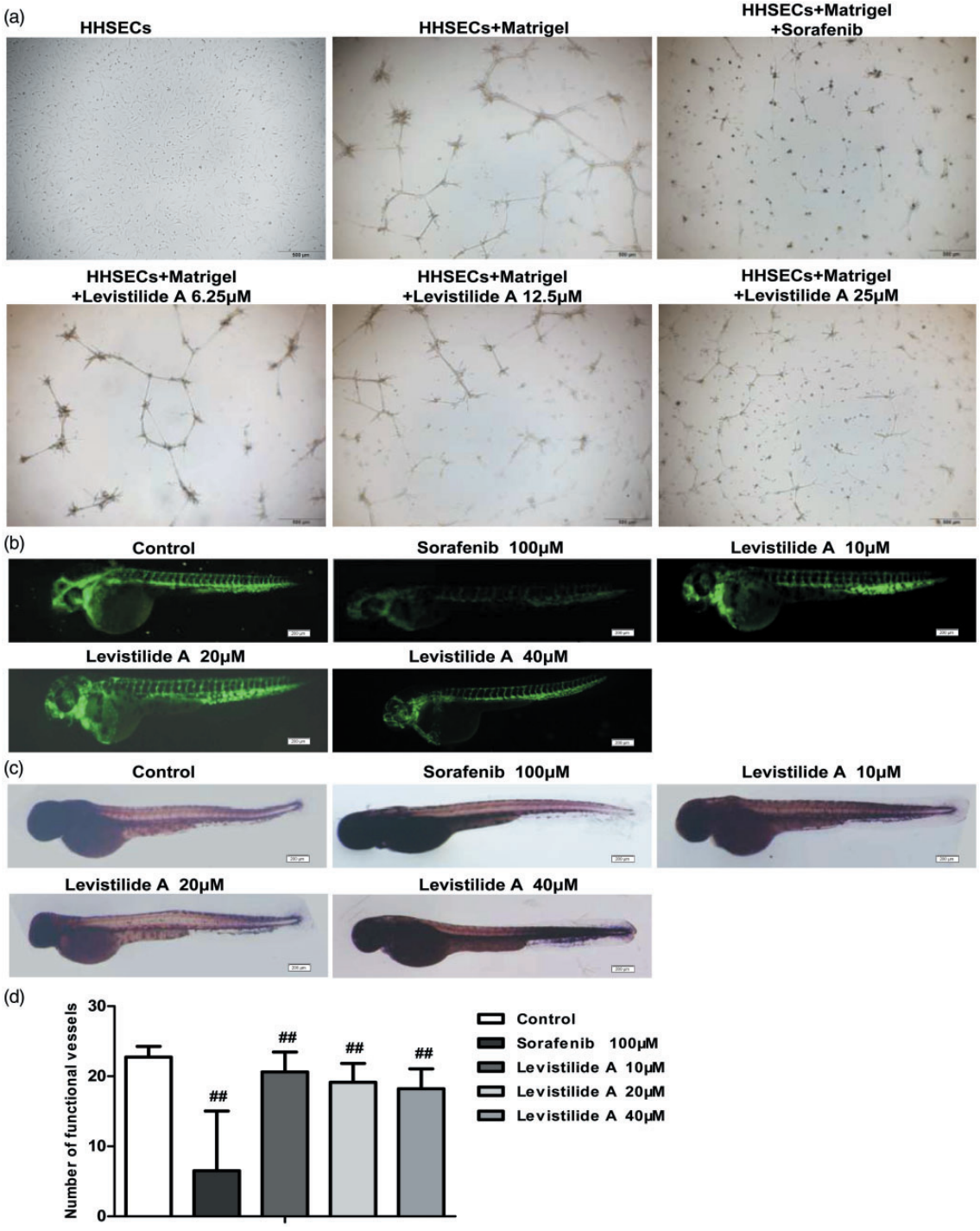

Figure 3 Levistilide A inhibited tube formation in Matrigel and the number of functional vessels in transgenic zebrafish. (a) Tube formation in Matrigel. Representative images were captured after incubation for 24 h (×100). (b) Observation of the intersegmental vessels of transgenic zebrafish (ISV) under stereo microscope. (c) Alkaline phosphatase staining of transgenic zebrafish. (d) Semi-quantification of the number of functional vessels in transgenic zebrafish. $^{\#\#}P < 0.01$, compared with control group. $n = 10$ per group. (A color version of this figure is available in the online journal.)

(80 and 100 μM; results not shown)-treated zebrafish. Levistilide A, at concentrations from 10 to 40 μM, significantly inhibited the number of ISVs with blood flow (Figure 3(b) and (d)). Alkaline phosphatase staining showed that the number of vessels in zebrafish embryos was significantly reduced (Figure 3(c)). These results indicated that levistilide A inhibited angiogenesis in zebrafish.

Effects of levistilide A on the organ index in CCl4-induced fibrotic rats

The body, liver, and spleen weights decreased significantly compared with normal control, whereas the ratio of liver or spleen weight to body weight increased significantly in CCl_4-treated rats. However, neither levistilide A (3 or 6 mg/kg/d) nor sorafenib (4 mg/kg/d) improved the organ index of CCl_4-treated rats (Table 2).

Table 2 Effects of levistilide A on the organ index in CCl4-induced fibrotic rats

Groups ($n = 10$)	Body weight (g)	Liver weight (g)	Spleen weight (g)	Liver/body weight ratio (%)	Spleen/body weight ratio (%)
Normal	343.20 ± 21.92	8.80 ± 0.82	0.61 ± 0.05	2.56 ± 0.11	1.76 ± 0.08
Model	164.40 ± 14.20**	9.36 ± 0.89	0.41 ± 0.06**	5.69 ± 0.29**	2.48 ± 0.33**
Sorafenib	158.67 ± 8.92	8.34 ± 1.17	0.43 ± 0.08	5.24 ± 0.53	2.76 ± 0.63
L 3 mg/kg	156.56 ± 16.62	8.70 ± 1.04	0.40 ± 0.04	5.60 ± 0.38	2.56 ± 0.26
L 6 mg/kg	174.11 ± 9.97	9.73 ± 1.04	0.46 ± 0.04	5.59 ± 0.56	2.63 ± 0.29

Data are mean ± SD. Liver fibrosis was induced mainly by subcutaneous injection of CCl_4 for six weeks and treated with 10 mL/kg of normal saline, 4 mg/kg/d of sorafenib, 3 and 6 mg/kg/d of levistilide A from the fourth week to the end of the experiment.
**$P < 0.01$, versus normal control.

Table 3 Levistilide A ameliorated serum liver function in CCl_4-induced fibrotic rats

Groups ($n = 10$)	ALT (IU/L)	AST (IU/L)	Alb (g/L)	T.Bil (μmol/L)
Normal	72.07 ± 7.19	62.04 ± 8.41	14.27 ± 0.75	6.20 ± 1.96
Model	405.81 ± 83.91**	286.95 ± 83.56**	7.14 ± 0.34**	9.12 ± 3.56**
Sorafenib	165.99 ± 70.07##	100.38 ± 29.17##	11.26 ± 0.56##	8.26 ± 1.55
L 3 mg/kg	399.99 ± 72.65	265.84 ± 88.74	9.77 ± 0.67##	9.58 ± 2.51
L 6 mg/kg	267.93 ± 52.03##	160.15 ± 69.62##	10.38 ± 1.38##	8.14 ± 1.66

Data are mean ± SD.
**$P < 0.01$, versus normal control; ##$P < 0.01$, versus model control.

Levistilide A ameliorated serum liver function in CCl4-induced fibrotic rats

The hepatic injury of CCl_4-treated rats was indicated by significantly higher AST, ALT, and TBil serum levels and a lower Alb concentration. However, levistilide A at 6 mg/kg reversed the increase of ALT and AST and the decrease of Alb, but had no significant effect on TBil, compared with control rats (Table 3).

Levistilide A alleviated liver fibrosis in CCl4-induced fibrotic rats

Sirius Red staining revealed dramatic collagen deposition in rats in the model group characterized by fibrous septa and cirrhotic nodules or pseudo lobules in liver tissue. In comparison, levistilide A-treated rats, especially those treated with 6 mg/kg of levistilide A, had slighter collagen accumulation (Figure 4(a) and (c)). The hepatic hydroxyproline (Hyp) content increased in CCl_4-treated rats, which, however, was reduced by 33.26 and 39.99% in rats treated with 3 and 6 mg/kg of levistilide A, respectively (Figure 4(d)). The protein expressions of collagen I and alpha smooth muscle actin (α-SMA), the HSC activation markers, were also observed to be downregulated compared with the model rats using the Western blot assay (Figure 4(b), (e), and (f)).

Levistilide A inhibited angiogenesis in CCl4-induced fibrotic rats

Liver microvessels were observed through synchrotron radiation 2D X-ray imaging (Figure 5(a)), vWF expression was detected through immunofluorescence (Figure 5(b)), sinusoidal fenestration was detected through SEM (Figure 6(a)), and basement membrane was observed through TEM (Figure 6(b)). The model rats had a larger number of new microvessels and higher vWF expression than control rats, but sinusoidal fenestration disappeared. However, levistilide A at both 3 and 6 mg/kg reduced the number of microvessels and the vWF expression and partly recovered the sinusoidal fenestration. Western blot results (Figure 7) showed that the expression of VEGF, VEGF receptor-2 (VEGF-R2), and CD31 was higher in model rats than in normal control rats. Levistilide A reduced the expression of CD31, VEGF, and VEGF-R2.

Discussion

Angiogenesis is a dynamic process including sprouting or intussusception from preexisting blood vessels, lumen formation, and stabilization of nascent vessels.[9] Liver has four vasculatures, the portal vein, hepatic artery, liver sinusoid, and hepatic vein. Exchange of substances between blood and parenchymal cells occurs in the liver sinusoid, a specific microvascular network in the liver.[10] During fibrosis, significant vascular remodeling occurs with increased SEC capillarization,[11] LSEC fenestration disappearance, continuous basement membrane formation, increased vWF expression,[12] and increased mural coverage of vessels by contractile HSCs.[13] Angiogenesis is probably a prerequisite step for fibrogenesis[14] and could be a surrogate marker for portal hypertension in liver diseases.[15] If fibrogenesis and angiogenesis are closely integrated and simultaneously occurring in the chronic liver diseases, intrahepatic circulation resistance would be increased. At the later stage of chronic liver injury, wound healing is less active and

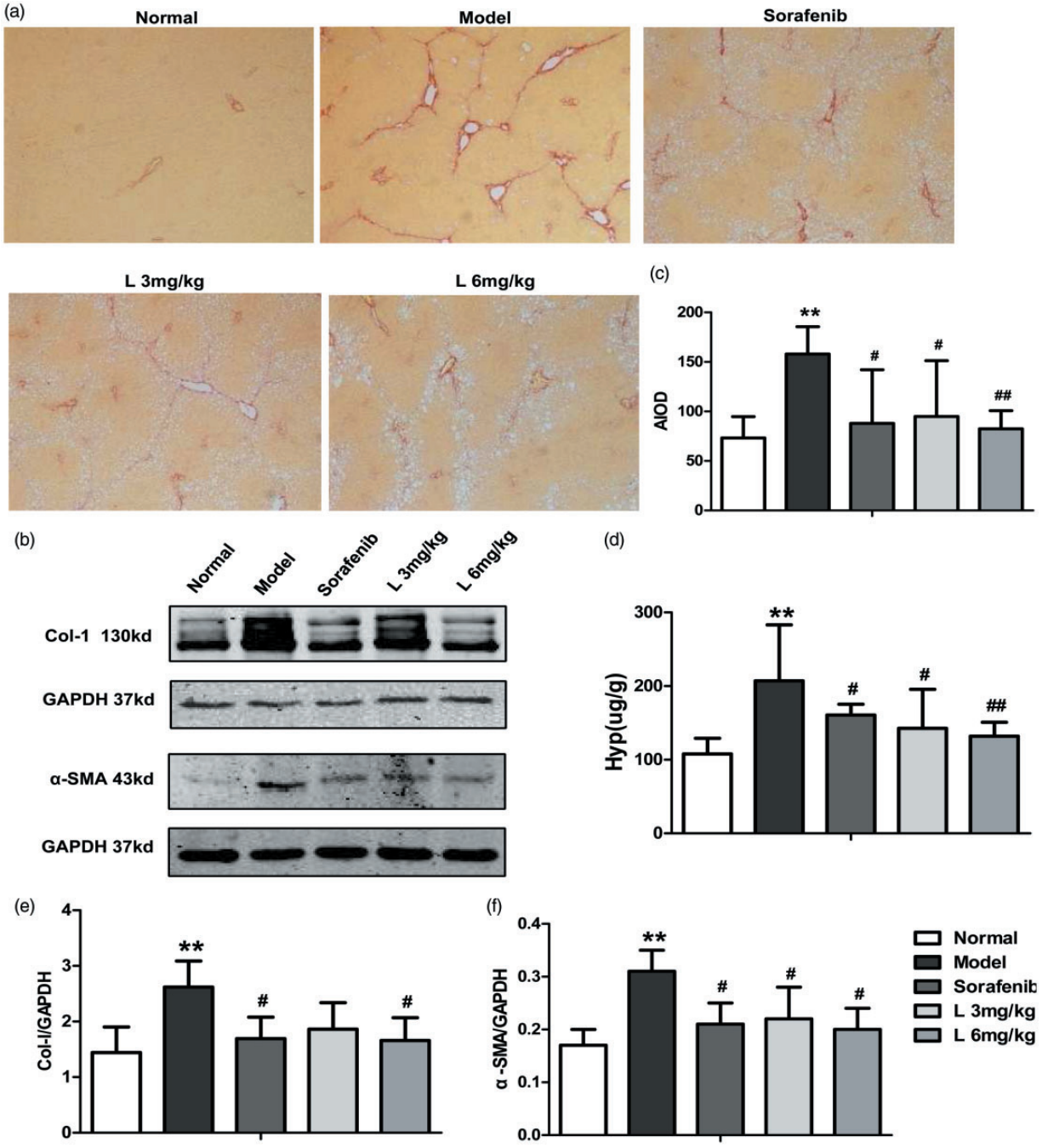

Figure 4 Effects of levistilide A on hepatic fibrosis in CCl_4-induced fibrotic rats. (a) Collagen deposition was revealed through Sirius Red staining (×100). (b) The protein expressions of collagen I and α-SMA were analyzed through Western blot. (c) Semi-quantification of Sirius Red staining was evaluated using the average integral optical density (AIOD). (d) Hyp content in the liver tissue was detected through the hydrochloric acid hydrolysis method. (e) Semi-quantification of collagen I protein expression. (f) Semi-quantification of α-SMA protein expression. $^{**}P < 0.01$, compared with normal control. $^{\#}P < 0.05$, $^{\#\#}P < 0.01$, compared with model control. $n = 10$ per group. Western blot data are presented from three independent experiments. (A color version of this figure is available in the online journal.)

fibrogenic transformation is more established, but persistent angiogenesis becomes part of fibrotic septa, particularly the larger and more mature fibrotic septa. Therefore, liver fibrosis reversal is difficult. Sinusoid capillarization is the cytological basis of pathological angiogenesis, and VEGF plays a predominant role in the initial stages of new blood vessel formation by stimulating endothelial cell proliferation and endothelial tubule formation. This is an important mechanism responsible for origination and development of liver fibrosis.[16] Therefore, regulating the VEGF signaling pathway and alleviating sinusoid capillarization are crucial in identifying therapeutic targets for vasculatures as well as fibrogenesis.

Visualization of microvasculatures is essential in investigating the mechanism of angiogenesis in liver fibrosis. The images of magnetic resonance angiography, computerized

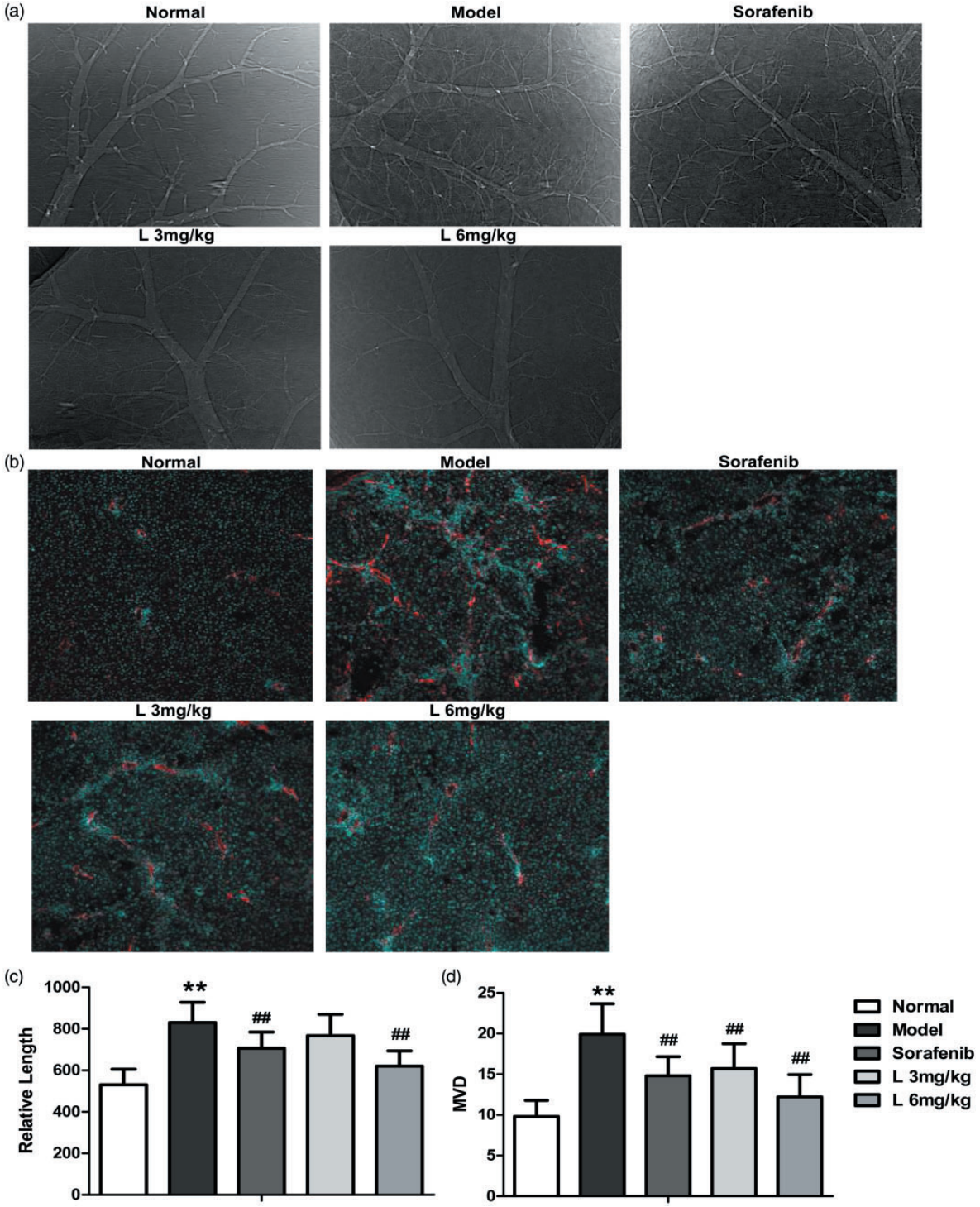

Figure 5 Influence of levistilide A on angiogenesis in CCl_4-induced fibrotic rats. (a) Liver microvasculature was examined through synchrotron radiation X-ray 2D imaging. (b) The expression of vWF was detected through immunofluorescence. (c) Semi-quantification data for microvasculature in X-ray 2D imaging were calculated and presented as relative length. (d) Microvessel density was determined as the mean number of vWF-positive labeled vessel sections in five successive high-magnification fields. $^{**}P < 0.01$, compared with normal control. $^{\#\#}P < 0.01$, compared with model control. $n = 10$ per group. (A color version of this figure is available in the online journal.)

tomographic angiography, and stereomicroscope are not adequate to display microvessels, such as sinusoid with a diameter less than 300 μM because of the limited resolution. However, synchrotron radiation combined with a high-resolution and high-speed imaging system has emerged as a powerful tool to visualize the microvessels of various animal organs,[17] enabling the detection of microcirculation in liver tissues. Vessels with a diameter of about 50 μM were distinguished in rat liver tissues by using synchrotron radiation X-ray interference.[18] Vessels with a diameter of 30 μM

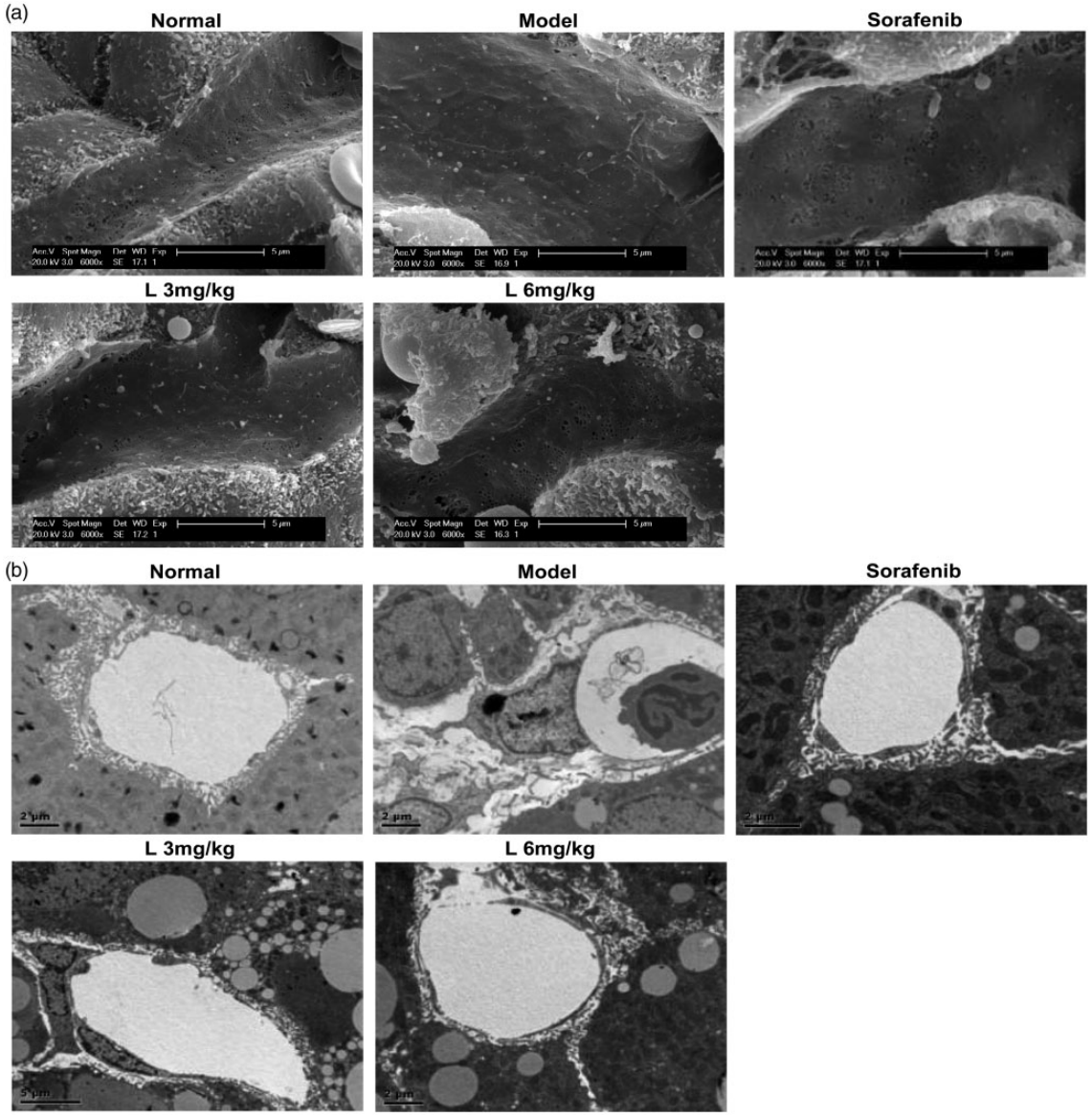

Figure 6 Influence of levistilide A on sinusoidal fenestration and basement membrane in CCl_4-induced fibrotic rats. (a) Sinusoidal fenestration was detected through a scanning electron microscope. (b) Basement membrane was observed through transmission electron microscope. $n = 10$ per group

were detected through angiography by using physiological saline as contrast agents.[19] This technology has been applied to visualize liver, brain,[20] and lung tumor[21] blood vessels. X-ray 2D imaging of liver microvessels by synchrotron radiation had a high concordance with the calculation of microvessel density with CD31 or vWF labeling.[22,23] Therefore, we selected synchrotron radiation X-ray 2D imaging as the main method for evaluating vasculatures.

In this study, we duplicated TGF-β1-induced LX-2 cell activation *in vitro*. Considering the overproliferation phenomenon of LSECs in sinusoid capillarization and liver fibrotic environment, the HHSEC model was induced by ECGS-containing VEGF. The ability of HHSECs to form tubelike structures was demonstrated using the tube formation assay. Zebrafish is an intact whole animal, which enables favorable gene analysis of vessel development. A zebrafish model is simple and rapid in evaluating angiogenesis, and hence suitable for large-scale screening and statistical analysis.[24] Therefore, we selected the four models as the primary method for vascular active drug screening in liver fibrosis. *In vivo*, liver fibrosis in rats was induced by subcutaneous CCl_4 injection and administrated with high-lipid and low-protein diets in this study. CCl_4 is a chemical reagent for free radical damage, which is converted to CCl_{3-} by cytochrome P450 and then caused lipid peroxidation.[25] The high-lipid and low-protein diets may promote the movement of lipid from body into the liver, and increase the hepatic lipid peroxidation induced by CCl_4. Because the model had the feature of oxidative stress injury[26] and angiogenesis, we selected this model to verify the activity of levistilide A and to further explain its antifibrosis mechanism. Levistilide A with high stability formed by ligustilide dimer could be converted into ligustilide in certain circumstances. The oral dosage for rats of

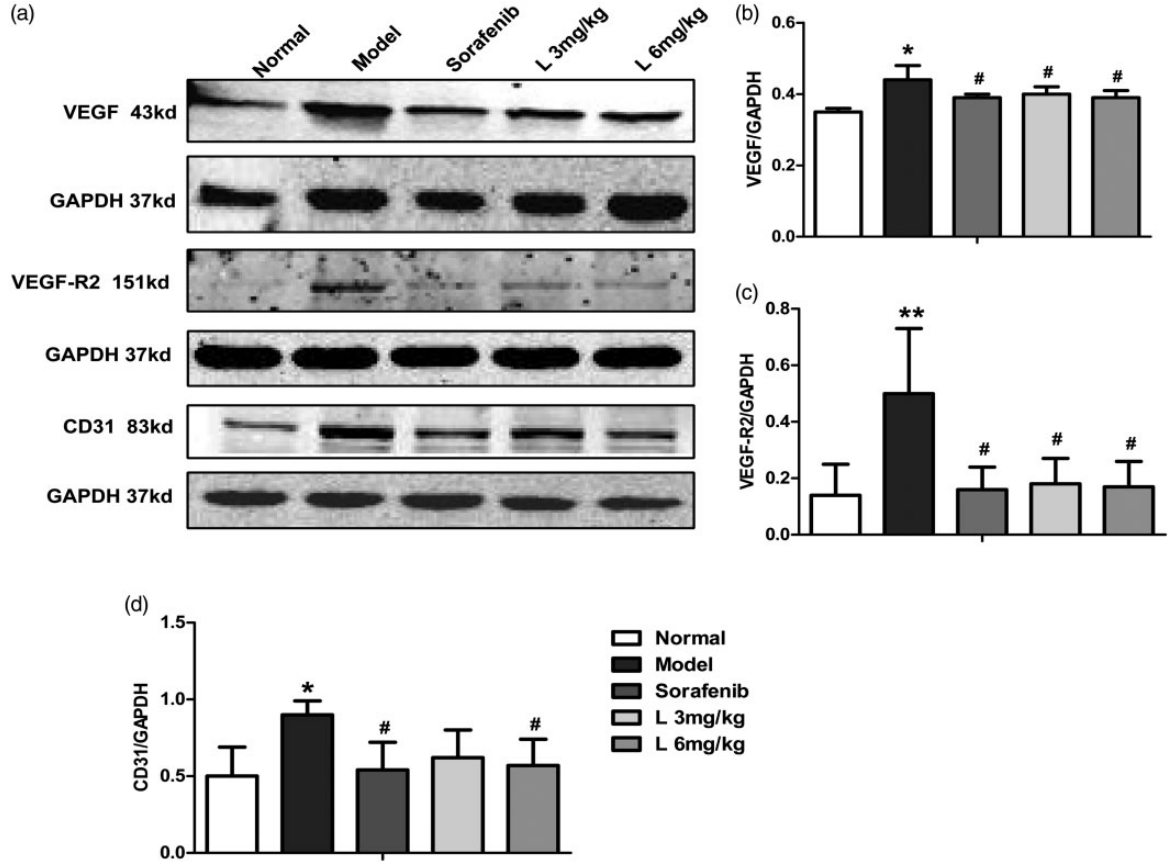

Figure 7 Influence of levistilide A on the expression of VEGF, VEGF-R2, and CD31 in CCl_4-induced fibrotic rats. (a) Western blot analysis revealed that levistilide A downregulated the expression of VEGF, VEGF-R2, and CD31. (b, c, d) Semi-quantification. $^{*}P < 0.05$, $^{**}P < 0.01$, compared with normal control. $^{\#}P < 0.05$, compared with model control. Data are presented from three independent experiments

ligustilide is 20–80 mg/kg according to the report.[27] The oral bioavailability of levistilide A is about 7.5% of one when it administrated by vein injection. Therefore, we calculated the higher injection dose $= 80 \times 7.5\% = 6$ mg/kg, and our pre-experiment showed that peritoneal injection of 6 mg/kg levistilide A has no obvious hepatotoxicity and was effective in liver fibrosis rats. So 3 and 6 mg/kg doses were administered in this study.

The results demonstrated that levistilide A and sorafenib inhibited the TGF-β1-induced LX-2 activation, confirmed the effectiveness of levistilide A on the activation of HSC as reported before. The effects of sorafenib on LX-2 cells were consistent with those reported in the literature.[28] Levistilide A inhibited ECGS-induced HHSEC proliferation, reduced the ability of HHSECs to form tubelike structures in Matrigel, and inhibited the number of functional vessels in transgenic zebrafish, indicating that levistilide A exhibited antiangiogenic activity at both cell and whole-animal levels. CCl_4 intoxication plus high fat food could induce liver inflammation, steatosis, fibrosis, and cirrhosis in rats, in severe case the animal model may develop into cirrhotic complications such as ascites.[29] Severe liver necroinflammatory or advance fibrotic animals often have lower serum Alb levels. In our study, animal model showed the hepatic inflammation and advanced fibrosis, with characteristics of elevated ALT/AST levels and decreased Alb content. While levistilide A showed an effect on liver inflammation by reducing ALT/AST levels in models, which may contribute to its antifibrotic effect. And the action mechanism of levistilide A on hypoalbuminemia is associated with its anti-inflammation and antifibrosis, also maybe implicated in improvement of sinusoidal circulation and hepatocyte nutrition and functions. Levistilide A ameliorated liver fibrosis in CCl_4-treated rats, downregulation of the Hyp content, and protein expression of collagen I and α-SMA. These results indicated that levistilide A inhibited the accumulation of ECM components and attenuated the activation of hepatic stellate. The antifibrosis effect of levistilide A is closely related to antiangiogenesis. We observed that levistilide A attenuated angiogenesis, reduced the number of new microvessels and vessel branches, and ameliorated sinusoid capillarization of liver tissues by improving fenestrations. The expression of vascular-related signaling molecules such as VEGF, VEGFR2, vWF, and CD31 was downregulated significantly. These results indicated that levistilide A attenuated liver angiogenesis by alleviating sinusoid capillarization related to the regulation of VEGF signaling pathways in fibrotic rats.

In conclusion, levistilide A inhibited LX-2 cell activation and HHSEC proliferation and exhibited significant antiangiogenesis activity. The animal liver fibrosis model confirmed that levistilide A reduced collagen deposition

and the number of microvessels; ameliorated sinusoid capillarization; and downregulated the expression of CD31, VEGF, and VEGF-R2. These findings suggest that levistilide A may be a potential drug for the treatment of liver fibrosis through antiangiogenesis, and this hypothesis must be verified by other fibrotic animal model studies or clinical trials.

Authorship contributions: CHL designed the project, ZMZ, HLL, XS, TG, and LS conducted the experiments, ZMZ and TG performed data analysis, YYT contributed the research methods and framework, and ZMZ wrote the paper.

ACKNOWLEDGEMENTS

This work was performed at beamline BL13W of the Shanghai Synchrotron Radiation Facility (SSRF), a third-generation synchrotron radiation facility. This work was supported by The National Natural Science Foundation of China (No. 81102702, 81473404, 81173405).

DECLARATION OF CONFLICTING INTERESTS

The author(s) declared no potential conflicts of interest with respect to the research, authorship, and/or publication of this article.

REFERENCES

1. Hernandez-Gea V, Friedman SL. Pathogenesis of liver fibrosis. *Annu Rev Pathol* 2011;**6**:425–56
2. DeLeve LD. Liver sinusoidal endothelial cells in hepatic fibrosis. *Hepatology* 2015;**61**:1740–6
3. Fernandez M, Semela D, Bruix J, Colle I, Pinzani M, Bosch J. Angiogenesis in liver disease. *J Hepatol* 2009;**50**:604–20
4. Thabut D, Routray C, Lomberk G, Shergill U, Glaser K, Huebert R, Patel L, Masyuk T, Blechacz B, Vercnocke A, Ritman E, Ehman R, Urrutia R, Shah V. Complementary vascular and matrix regulatory pathways underlie the beneficial mechanism of action of sorafenib in liver fibrosis. *Hepatology* 2011;**54**:573–85
5. Lee TF, Lin YL, Huang YT. Studies on antiproliferative effects of phthalides from *Ligusticum chuanxiong* in hepatic stellate cells. *Planta Med* 2007;**73**:527–34
6. Wang F, Wang F, Zou Z, Liu D, Wang J, Su Y. Active deformation of apoptotic intestinal epithelial cells with adhesion-restricted polarity contributes to apoptotic clearance. *Lab Invest* 2011;**91**:462–71
7. Lv J, Zhao Z, Chen Y, Wang Q, Tao Y, Yang L, Fan TP, Liu C. The Chinese herbal decoction *Danggui buxue* tang inhibits angiogenesis in a rat model of liver fibrosis. *Evid Based Complement Alternat Med* 2012;**2012**:284963
8. Peng Y, Chen Q, Yang T, Tao Y, Lu X, Liu C. Cultured mycelium *Cordyceps sinensis* protects liver sinusoidal endothelial cells in acute liver injured mice. *Mol Biol Rep* 2014;**41**:1815–27
9. Lee JS, Semela D, Iredale J, Shah VH. Sinusoidal remodeling and angiogenesis: a new function for the liver-specific pericyte? *Hepatology* 2007;**45**:817–25
10. Brunt EM, Gouw AS, Hubscher SG, Tiniakos DG, Bedossa P, Burt AD, Callea F, Clouston AD, Dienes HP, Goodman ZD, Roberts EA, Roskams T, Terracciano L, Torbenson MS, Wanless IR. Pathology of the liver sinusoids. *Histopathology* 2014;**64**:907–20
11. Straub AC, Stolz DB, Ross MA, Hernandez-Zavala A, Soucy NV, Klei LR, Barchowsky A. Arsenic stimulates sinusoidal endothelial cell capillarization and vessel remodeling in mouse liver. *Hepatology* 2007;**45**:205–12
12. Sarin SK, Brenner DA, Jolla L. Postgraduate course: integrating basic science into clinical practice. *Hepatol Int* 2010;**4**(Suppl 1):S1–S85
13. Xie G, Wang X, Wang L, Wang L, Atkinson RD, Kanel GC, Gaarde WA, Deleve LD. Role of differentiation of liver sinusoidal endothelial cells in progression and regression of hepatic fibrosis in rats. *Gastroenterology* 2012;**142**:918–27.e6
14. Yang L, Kwon J, Popov Y, Gajdos GB, Ordog T, Brekken RA, Mukhopadhyay D, Schuppan D, Bi Y, Simonetto D, Shah VH. Vascular endothelial growth factor promotes fibrosis resolution and repair in mice. *Gastroenterology* 2014;**146**:1339–50.e1
15. Hu DD, Habib S, Li XM, Wang TL, Wang BE, Zhao XY. Angiogenesis: a new surrogate histopathological marker is capable of differentiating between mild and significant portal hypertension. *Histol Histopathol* 2015;**30**:205–12
16. Liu P. Inhibition of pathological angiogenesis of Chinese medicine against liver fibrosis. *Chin J Integr Med* 2016;**22**:569–72
17. Mori H, Hyodo K, Tanaka E, Uddin-Mohammed M, Yamakawa A, Shinozaki Y, Nakazawa H, Tanaka Y, Sekka T, Iwata Y, Handa S, Umetani K, Ueki H, Yokoyama T, Tanioka K, Kubota M, Hosaka H, Ishikawa N, Ando M. Small-vessel radiography in situ with monochromatic synchrotron radiation. *Radiology* 1996;**201**:173–7
18. Momose A, Takeda T, Itai Y. Blood vessels: depiction at phase-contrast X-ray imaging without contrast agents in the mouse and rat-feasibility study. *Radiology* 2000;**217**:593–6
19. Takeda T, Momose A, Wu J, Yu Q, Zeniya T, Thet-Thet-Lwin, Yoneyama A, Itai Y. Vessel imaging by interferometric phase-contrast X-ray technique. *Circulation* 2002;**105**:1708–12
20. Guan Y, Wang Y, Yuan F, Lu H, Ren Y, Xiao T, Chen K, Greenberg DA, Jin K, Yang GY. Effect of suture properties on stability of middle cerebral artery occlusion evaluated by synchrotron radiation angiography. *Stroke* 2012;**43**:888–91
21. Liu X, Zhao J, Sun J, Gu X, Xiao T, Liu P, Xu LX. Lung cancer and angiogenesis imaging using synchrotron radiation. *Phys Med Biol* 2010;**55**:2399–409
22. Randi AM, Laffan MA, Starke RD. Von Willebrand factor, angiodysplasia and angiogenesis. *Mediterr J Hematol Infect Dis* 2013;**5**:e2013060
23. Sharma B, Singh N, Gupta N, Lal P, Pande S, Chauhan S. Diagnostic modalities of precancerous and cancerous cervical lesions with special emphasis on CD31 angiogenesis factor as a marker. *Patholog Res Int* 2013;**2013**:243168
24. Marone G, Granata F. Angiogenesis, lymphangiogenesis and clinical implications. *Preface.* Chem Immunol Allergy 2014;**99**:XI–XII
25. Weber LW, Boll M, Stampfl A. Hepatotoxicity and mechanism of action of haloalkanes: carbon tetrachloride as a toxicological model. *Crit Rev Toxicol* 2003;**33**:105–36
26. Tipoe GL, Leung TM, Liong EC, Lau TY, Fung ML, Nanji AA. Epigallocatechin-3-gallate (EGCG) reduces liver inflammation, oxidative stress and fibrosis in carbon tetrachloride (CCl4)-induced liver injury in mice. *Toxicology* 2010;**273**:45–52
27. Wu XM, Qian ZM, Zhu L, Du F, Yung WH, Gong Q, Ke Y. Neuroprotective effect of ligustilide against ischaemia-reperfusion injury via up-regulation of erythropoietin and down-regulation of RTP801. *Br J Pharmacol* 2011;**164**:332–43
28. Hong F, Chou H, Fiel MI, Friedman SL. Antifibrotic activity of sorafenib in experimental hepatic fibrosis: refinement of inhibitory targets, dosing, and window of efficacy in vivo. *Dig Dis Sci* 2013;**58**:257–64
29. Domenicali M, Caraceni P, Giannone F, Baldassarre M, Lucchetti G, Quarta C, Patti C, Catani L, Nanni C, Lemoli RM, Bernardi M. A novel model of CCl4-induced cirrhosis with ascites in the mouse. *J Hepatol* 2009;**51**:991–9

(Received October 18, 2016, Accepted February 24, 2017)